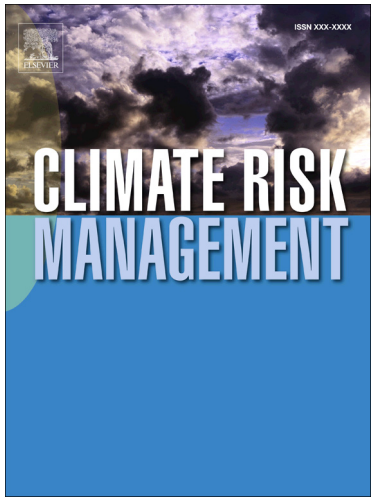

Assessment of risks due to climate change for the Upper Tamakoshi Hydropower Project in Nepal

Sangam Shrestha, Ajay Ratna Bajracharya, Mukand S. Babel

PII: S2212-0963(16)30027-4
DOI: http://dx.doi.org/10.1016/j.crm.2016.08.002
Reference: CRM 80

To appear in: *Climate Risk Management*

Received Date: 12 July 2015
Revised Date: 23 June 2016
Accepted Date: 4 August 2016

Please cite this article as: S. Shrestha, A.R. Bajracharya, M.S. Babel, Assessment of risks due to climate change for the Upper Tamakoshi Hydropower Project in Nepal, *Climate Risk Management* (2016), doi: http://dx.doi.org/10.1016/j.crm.2016.08.002

Assessment of risks due to climate change for the Upper Tamakoshi Hydropower Project in Nepal

Sangam Shrestha*, Ajay Ratna Bajracharya, Mukand S. Babel

Water Engineering and Management, School of Engineering and Technology, Asian Institute of Technology, P.O. Box 4, Klong Luang, Pathum Thani 12120, Thailand

*Corresponding Author: Dr. Sangam Shrestha

Tel: +66-847284535, e-mail: sangam@ait.asia and sangamshrestha@gmail.com

Abstract

Climate change poses significant challenges to hydropower development and management in mountainous basins. This study examined the impact of climate change, and the associated risks, on the energy production of the Upper Tamakoshi Hydropower Project, which is located in the Tamakoshi basin of Nepal. The outputs of three GCMs—namely MIROC-ESM, MRI-CGCM3, and MPI-ESM-M—under the Representative Concentration Pathways (RCP) scenarios were used for the projection of precipitation and temperature in the future. The minimum and maximum temperatures of the basin are projected to increase by 6.33 ºC and 3.82 ºC, respectively, by 2100. The projected precipitation varies from -8% to +24.8%, which is expected to alter the streamflow by -37.83% to +47% in the future. Based on the streamflow output, the risk for energy production was calculated with respect to the baseline energy production of 1963 GWh and 2281 GWh. Using the three GCMs, the risk associated with annual hydropower production under altered runoff was analyzed. The risk percentage in the future periods shows a mild risk varying from 0.69 % to 6.63%. MPI-ESM-M GCM

projects a higher percentage of risk for energy production during the same future periods, as compared to the baseline energy production of 1963 GWh. A mild to moderate risk of 13.24% can be expected when energy production in the future is compared to the baseline energy production of 2281 GWh.

Keywords: Tamakoshi basin, Climate Change, Hydrology, Hydropower, Risk

1. Introduction

The climate of the Earth has been evolving and changing continuously over millions of years. However, the rate of change in climate in the 21st century has scientists alarmed. The Industrial Revolution began in the 1800s, which led to extensive use of fossil fuels and natural resources (Baede et al., 2001). This trend of development progressed with the advancement in new technologies and new inventions, with which began rapid global urbanization, ultimately leading to the extensive and indiscriminate use of fossil fuels (Baede et al., 2001). Since the 1800s, carbon dioxide concentrations have been rapidly increasing: from 280 ppm to a record breaking concentration of 400 ppm in May 2013 (Bala, 2013). By the end of the 21st century, the global surface temperature is expected to exceed by 1.5 ºC relative to 1850 to 1900 for all RCP scenarios except RCP 2.5 (Stocker et al., 2013). The IPCC report shows that global temperature is expected to exceed by 2 ºC for scenarios RCP 6.0 and RCP 8.5.

Climate change causes a rise in global temperature, which can have tremendous impact on global water cycles and precipitation patterns. These impacts cause important changes in the management of water, particularly on uses highly dependent on the hydrological regime, such

as hydropower production. Nepal has a huge potential for hydropower generation due to its topography, landscape, and abundant water resources. The first technical analysis of the hydropower potential of Nepal was carried out in 1966. This report estimated a theoretical capacity of 83,000 MW and an economic capacity of 42,000 MW (Shrestha, 2015). The history of hydropower production in Nepal is more than a hundred years old. However, the actual development of hydropower in Nepal does not quite match up as the current power production from hydropower is merely 718 MW, with 43 hydropower plants under operation (DOED, 2015).

Nepal has a subtropical monsoon climate. The elevation in Nepal varies from 60 m above sea level (masl) in the south to 8850 masl to the north. Temperature and precipitation, along with other climatic variables, change with differences in elevation due to which Nepal has diverse climate conditions, ranging from a tropical climate in the south to an alpine climate in the higher northern regions (Shrestha and Aryal, 2011).

A study carried out in the Koshi basin shows an increase in the projected precipitation during the 2030s and 2050s under A2 and B1 scenarios in most of the upper sub-basins, whereas the lower sub-basins are expected to experience a decrease in precipitation during the 2030s (Bharati et al., 2014). Temporal and spatial variations in temperature and precipitation can directly influence the water resources and the hydrology of the basin. A recent study of the Bagmati River basin of Nepal showed the potential impact of future climatic conditions on the hydrology of the region. The projection showed an increase in the temperature of the basin, with a significant increase in summer temperature under A2 and B2 scenarios (Babel et al., 2013). The projection showed an increase of up to 12.84%, in the future, in the basin's average annual water availability. The impact of climate change is even more evident in those

Himalayan regions where glaciers are retreating at an alarming rate due to global warming. Shea et al. (2014) carried out simulations of future glacier changes based on RCP scenarios in the Everest region using a glacier mass balance model. Their study revealed that the glaciers are not only affected by the changes in temperature but also by the equilibrium line altitude (ELA) (Shea et al., 2014). The volume of these glaciers is projected to reduce by up to 62% by the 2050s. The maximum loss in glacier volume—up to 96%—can be expected by the end of the century, if the projection of temperature in the future is accurate (Shea et al., 2014).

It is evident that the precipitation patterns and temperature, as well as other climatic variables, are changing and are expected to change in the future as well. The operation of a hydropower plant depends on several climatic factors and is sensitive to changes in climate variables (Robinson, 1997). A study carried out at the Kulekhani Hydropower Project (60 MW) in Nepal revealed the influence of climate change on the hydrology of a basin and its consequent effects on electricity production. The study showed a decrease in power production by up to 30% when electricity is generated for seven hours a day. Hydropower production was found to decrease by up to 13% when the hydropower plant is driven for ten hours a day during the dry season and three hours a day during the wet season (Shrestha et al., 2014).

Several studies on the risk analysis in construction projects have been carried out but very few studies have concentrated on the impact of climate change on renewable energy projects like hydropower plants. Mimikou and Baltas (1997) conducted a risk assessment of the storage type of a hydropower plant using climate change scenarios. In their study, risk analysis was carried out by calculating the percentage of failure of energy production and volume of storage. Failure was considered to have occurred when the monthly volume or the

energy production was less than expected or less than the minimum guaranteed energy production (Mimikou and Baltas, 1997).

The present study aims at quantifying the risk percentage associated with energy production at the Upper Tamakoshi Hydropower Project in Nepal with respect to the impact of climate change under the new RCP scenarios. The study can be of significant importance as run-of-the-river type of hydropower plants are more susceptible to climate change in a snow-fed river basin and most of the hydropower plants in Nepal are based on the run-of-the-river design.

2. Study Area's Characteristics

The study was carried out in the Tamakoshi basin of Nepal, which is one of the sub-basins of the Koshi basin (Fig. 1). It extends from 27° 37' 42" to 28° 19' 23" in the north and from 86° 0' 9" to 86° 34' 12" in the east. The Tamakoshi basin extends from the High Himalayan to the Siwalik range, ranging from an elevation of 849 masl to 7315 masl with a total area of 2926 km^2 (Khadka et al., 2014). The project's area and the Tamakoshi River are located in the eastern region, together with the neighboring rivers: Bhotekoshi (to the west) and Dudhkoshi (to the east). Tamakoshi is a tributary of the Sunkoshi River, which joins the Arun and Tamor Rivers to form the final Sapta Koshi section. Like other trans-Himalayan catchments, the upper region of the Tamakoshi catchment is partially protected from monsoon rainfall in the summer months. Temperature data obtained from the Jiri station, which is the nearest temperature station to the project area, indicates a summer (June to August) maxima of 25º C and a winter (December to February) minima of -2º C.

The Upper Tamakoshi Hydropower Project (456 MW) is the largest hydropower project under construction in Nepal. The project is located in the Dolakha district of Nepal at latitudes 27º 50' to 28º 00' N and longitudes 86º 10' to 86º 15' E. The project lies near the lower region of the Higher Himalayas. Upper Tamakoshi is a peaking run-of-the-river type of hydropower (PROR) plant with design discharge of 66 m^3/s. A maximum gross head of 822 m will be utilized to produce electricity from four Pelton turbines.

Fig. 1. Location map of the Tamakoshi basin with its hydrological and meteorological stations.

3. Materials and Methodology

The methodology adopted for this study is depicted in Fig. 2. GIS data such as DEM, land use, and soil map were used as spatial data to set up the Soil and Water Assessment Tool (SWAT model). Observed temperature and precipitation—along with other climatic variables such as relative humidity, solar radiation, and wind speed—were used to simulate the streamflow. The setup of the SWAT model was followed by the calibration and validation of the model based on observed streamflow at the Lamabagar and Busti stations. Streamflow was projected for the future period by using the temperature and precipitation projected on the basis of the quantile mapping method. The projected temperature and precipitation acted as input for the validated SWAT model. The outputs of the three chosen General Circulation Models (GCMs), MIROC-ESM, MRI-CGCM3, and MPI-ESM-M, were used to project future climate scenarios. The streamflow obtained from the SWAT model was used for the risk assessment of the impact of climate change on hydropower generation in the study area.

Fig. 2. The methodology adopted for the study.

3.1 Spatial GIS Data

DEM was used to get information on the elevation of any point in a given area at a specific spatial resolution. For this study, ASTER DEM of 30m resolution was used to delineate the watershed and to generate the streamflow pattern of the terrain.

The textural and physio-chemical properties of different layers of each soil type are necessary for input in a SWAT model. The soil data were obtained from SOTER (Soil and Terrain Database Programme) for Nepal and China at a scale of 1:1 million.

A land use map of the study area was obtained from the European Space Agency website (http://www.esa.int/ESA). The land use maps of 2004 and 2009 with resolutions of 300m were used.

3.2 Climatic Data

The hydrological and meteorological data of the basin were collected from the Department of Hydrology and Meteorology (DHM), Nepal. DHM has recorded data of two meteorological stations in the Tamakoshi basin: Charikot and Jiri. Table 1 shows the stations of the Tamakoshi basin which were used for the analysis of the hydrological and meteorological data.

Table 1 Hydro-meteorological stations in the Tamakoshi basin used in the study.

3.3 Downscaling of GCM data

Different GCMs, which are used in the Coupled Model Intercomparison Project phase 5 (CMIP5), based on Representative Concentration Pathways (RCP) scenarios, were analyzed for the selection of a suitable GCM to downscale precipitation and temperature variables for the Tamakoshi basin. The suitability of the GCMs was based on mainly three statistical parameters: standard deviation (SD), root mean square error (RMSE), and coefficient of determination (R^2). Three GCMS, MIROC-ESM, MRI-CGCM3, and MPI-ESM-M, were found to be statistically reliable in simulating the observed climatic data and hence were used further for the downscaling of temperature and precipitation. Table 2 provides a detailed description of the GCMs, which have different resolutions, used in this study.

Table 2 GCMs, their sources, resolutions, vintage and data sources used in the study.

The quantile mapping technique was used to downscale the GCMs' data to the basin level. Quantile mapping is based on matching the two cumulative distribution functions (CDFs) of the GCMs' simulated and observed data. In this method, the quantile value of the cumulative distribution function of temperature or precipitation is matched with the consequent quantile value of the cumulative distribution function of the GCM's simulated variable (Hamlet et al., 2010). The statistical transformation in quantile mapping is represented by Equations 1 and 2 (Gudmundsson et al., 2012).

The statistical transformation can be represented as:

$$P_0 = h(P_G) \tag{1}$$

The transformation is defined as:

$$P_0 = F_0^{-1}(F_G(P_G)) \tag{2}$$

where F_G is the CDF of P_G and F_0^{-1} is the inverse CDF corresponding to P_0

3.4 Hydrological Modeling

The Soil and Water Assessment Tool (SWAT) model was used to simulate daily streamflow at the outlet and to predict the future runoff of the basin. There are two methods to estimate surface runoff in a SWAT model: i) USDA Soil Conservation Service, and ii) the Green and Ampt Infiltration method. In this study the SCS curve number method was adopted to estimate surface runoff.

The surface runoff from the SCS curve number is represented using the following equation (USDA, 1969):

$$Q_{surf} = \frac{(R_{day} - 0.2S)^2}{(R_{day} + 0.8S)} \tag{3}$$

where Q_{surf} is the accumulated runoff (mm); R_{day} is the rainfall depth for the day (mm); and S is the retention parameter (mm)

USDA (1969) gave the retention parameter as:

$$S = 25.4\left(\frac{100}{CN}\right) - 10 \tag{4}$$

where CN is the SCS curve number

Snowmelt was included with rainfall in the calculations of runoff and percolation. Snowmelt is represented using following equation (Neitsch, 2009):

$$SNO_{mlt} = b_{mlt} - sno_{\text{cov}}\left(\frac{T_{snow} + T_{mlt}}{2}\right) - T_{mlt} \tag{5}$$

where SNO_{mlt} is the amount of snowmelt on a given day (mm); B_{mlt} is the melt factor for the day (mm/day℃); and T_{mlt} is the base temperature above which snowmelt is allowed (℃)

The model's performance in simulating streamflow was evaluated using three statistical indicators recommended by Moriasi et al. (2007): Nash-Sutcliffe efficiency (NSE), percent bias (PBIAS), and ratio of the root mean square error to the standard deviation of measured data (RSR). The performance analysis of the model in this study was based on these three parameters, and an additional parameter of the correlation coefficient (R^2).

$$R^2 = \frac{n\sum xy - \sum x \sum y}{\left(\sqrt{n(\sum x^2) - (\sum x)^2}\right) \times \left(\sqrt{n(\sum y^2) - (\sum y)^2}\right)} \quad (6)$$

where x is the observed value and y is the simulated value

$$PBIAS = \frac{\sum_i^n (Yiobs - Yisim) \times 100}{\sum_i^n Yiobs} \quad (7)$$

where *Yiobs* is the observed data and *Yisim* is the model's simulated data

$$NSE = 1 - \frac{\sum_{i=1}^n (Q_i - Q_i')^2}{\sum_{i=1}^n (Q_i - \overline{Q_i})^2} \quad (8)$$

where Q_i is the measured daily streamflow, Q_i' is the simulated daily streamflow, $\bar{Q}_i$ is the average daily streamflow for the simulation period, and n is the number of daily streamflow values.

$$RSR = \frac{RMSE}{STDEV^{obs}} = \frac{\sqrt{\sum_{i=1}^n (Yiobs - Yisim)^2}}{\sqrt{\sum_{i=1}^n (Yiobs - Ymean)^2}} \quad (9)$$

3.5 Impact of Climate Change on Hydropower Production

The Upper Tamakoshi Hydropower Project is a peaking run-of-the-river type of hydropower plant. Energy production during the dry and wet periods depends upon the availability of

water in the river. To analyze the impact of climate change on the energy production from the hydropower plant, first a SWAT model was used to simulate the streamflow for a historical period: from 1975 to 2004. The streamflow obtained from the SWAT model was used as the baseline to analyze the impact of future changes in precipitation and temperature obtained after the bias correction of GCM data. The impact of climate change on power generation was analyzed for three time windows: the 2030s (2015 – 2039), the 2060s (2040 – 2069), and the 2090s (2070 – 2099).

Hydropower (electrical power) is calculated using the following equation:

$$W = \eta \times \gamma \times Q \times H \tag{10}$$

where η is the dimensionless efficiency of a turbine, ϒ is the specific weight of water, Q is the flow in cubic meters per second, and H is the net head

$$H = H_g - l_m \left(\frac{Q}{Qm} \right)^2 \tag{11}$$

where H_g is the gross head in meters, l_m is the length of the waterway, Q is the actual water flow, and Qm is the designed water flow

Annual Energy production in KWh can be calculated using Equation 12:

$$\text{Annual Energy (KWh)} = \text{Power (KW)} \times \text{hours in a day} \times \text{days in a year} \tag{12}$$

3.6 Risk Analysis

In this study, risk analysis was carried out by varying the annual energy production (E) within a specified range. The annual energy production was chosen to vary between the minimum

guaranteed energy production of 824.9 GWh obtained from the minimum streamflow of 13.6 m^3/s to 1961 GWh, obtained at the mean average annual streamflow of 60 m^3/s. Risk analysis was carried out for projections of future climate as per the three GCMs mentioned earlier: MIROC-ESM, MRI-CGCM3, and MPI-ESM-M under RCP 4.5 and RCP 8.5 scenarios. The risk analysis was carried out for three timeline periods: the 2030s (2015 – 2039), the 2060s (2040 – 2069), and the 2090s (2070 – 2099).

Failure or risk value was calculated for each scenario, equal to the relative percentage of the frequency of monthly failures within the series. A risk is considered to occur when the monthly energy E does not the follow the constraints given in Equation 13. The risk associated with the given E was calculated for each GCM and the different timeline periods for RCP 4.5 and RCP 8.5 scenarios. For no risk to occur, the energy E_t, produced during the month t, must be greater than the guaranteed or designed value (Mimikou and Baltas, 1997).

$$b_t E \leq E_t \tag{13}$$

where E is the annual energy production (GWh); E_t is the energy (GWh) produced during month t; and b_t is the monthly distribution coefficient of the observed/designed annual energy production. The monthly distribution coefficient was calculated for each month based on the mean value of energy production during the design period.

The Tamakoshi Hydropower Project is currently under construction. 2281 GWh was considered as the baseline annual power production, which is also the intended power production as per the design of the project. This value was estimated based on the daily discharge data of 5 years in the feasibility study of the project. In addition, to address the variability in discharge, power production was estimated based on 30 years of discharge data. The estimated hydropower production is 1963 GWh.

4. Results and Discussion

4.1 Bias Correction

Bias correction of the precipitation and temperature of the historical period was done before projecting future rainfall and temperature from the selected GCMs. The historical rainfall and temperature data from MRI-CGCM3, MIROC-ESM, and MPI-ESM-M were bias corrected for the observed stations of Charikot and Jiri. The rainfall and temperature data for the period of 30 years, from 1975 to 2004, were used for bias correction using the quantile mapping method (Hamlet et al., 2010; Wood et al., 2004). Table 3 and Table 4 illustrate the evaluation of the quanitle mapping method based on the three statistical parameters—SD, R^2, and RMSE—for the Charikot station and the Jiri station respectively.

Table 3 Evaluation of bias correction for precipitaiton data of MIROC-ESM, MRI-CGCM3, and MPI-ESM-M GCMs for the Charikot station.

Table 4 Evaluation of bias correction for precipitation, minimum temperature, and maximum temperature data of MIROC-ESM, MRI-CGCM3, and MPI-ESM-M GCMs for the Jiri station.

The simulated temperature from the GCMs had a much better resemblence to the observed temperature than the simulated to observed match in the case of precipitation. However, the correlation of maximum temperature of MPI-ESM-M was found to be only 0.55 before bias correction and 0.69 after bias correction. Minimum temperatures for all stations were found to have correlation coefficients greater than 0.9 for all three GCMs. The correlation coefficient of maximum temperature after bias correction varied from 0.69 to 0.85. All the three GCMs showed significant biases with respect to the observed precipitation and

temperature before bias correction. Wet seasons were under-projected by the GCMs whereas some dry seasons were over-projected. Both the wet season biases and dry season biases of precipitation were corrected after bias correction of the GCMs' data.

4.2 Projection of Precipitation and Temperature

For the projection of precipitation and temperature in the future, GCM data from 2015 to 2099 were used after bias correction. The future time period was divided into 3 timelines of 30 years' interval each: the 2030s (2015 – 2039), the 2060s (2040 – 2069), and the 2090s (2070 – 2099). MIROC-ESM and MRI-CGCM3 show increases in annual precipitation for both RCP 4.5 and RCP 8.5 scenarios except MIROC-ESM predicts a decrease in precipitation by 0.7% and 2.1% during the 2030s for the Charikot station and the Jiri station, respectively, for the RCP 4.5 scenario. . However, the patterns of precipitation change seasonally and are different for different GCMs. For the Charikot station, the projection shows an increase in precipitation for MIROC-ESM and MRI-CGCM3 whereas MPI-ESM-M shows a decrease in future precipitation (Fig. 3). The range of change in annual precipitation for all the three GCMs under the two RCP scenarios varies from -9.9% to +24.8%. Monsoon precipitation (June, July, August) is expected to be more intense, with projections ranging from an increase by 3.4% (MIROC-ESM, RCP 4.5) up to 20.7% (MRI-CGCM3, RCP 8.5). Monsoon rainfalls are projected to decrease in case of MPI-ESM-M. The bias corrected MIROC-ESM and MPI-ESM-M precipitations show decreasing projection during the dry season as well. The MRI-CGCM3 projection shows an increase in precipitation for all the seasons, with an average annual increase in precipitation by 10.1% and 14.5% for RCP 4.5 and RCP 8.5 scenarios respectively.

Fig. 3. Percentage change in future projected precipitation at the Charikot station with respect to the baseline period (1975 – 2004) for different GCMs.

For the Jiri station, MIROC-ESM and MRI-CGCM3's projections show an increase in annual precipitation, whereas MPI-ESM-M shows a decrease in the annual average precipitation except for a slight increase of 0.9% during the 2090s under the RCP 4.5 scenario. The projection of precipitation of MRI-CGCM3 shows an increase in annual average rainfall for all seasons except for the spring season where there are decreases of 12.9% and 11.8% for RCP 4.5 and RCP 8.5 scenarios respectively (Fig. 4). Similarly, an increase in wet season precipitation and decrease in some dry season precipitation is expected from MIROC-ESM and MRI-CGCM3. Both wet and dry seasons' precipitations are expected to decrease under MPI-ESM-M's projection. The maximum decrease in precipitation is expected to occur during the spring of the 2030s: by 19.7% under the RCP 4.5 scenario; the maximum increase, by 41.7%, is expected to occur during the autumn of the 2090s under the RCP 8.5 scenario.

Fig. 4. Percentage change in projected precipitation for the future at the Jiri station with respect to the baseline period (1975 – 2004) for different GCMs.

Minimum temperature as well as maximum temperature are subject to increase in the future, as projected by all three GCMs. Temperature at the Jiri station is expected to rise by 0.22 ºC to 1.58 ºC during the 2030s. In the 2060s, an increase in temperature by 0.83 ºC to 3.6 ºC is expected; however, the maximum rise in temperature is projected to increase by 1.39 ºC to 6.33 ºC in 2090s (Fig. 5). Increase in minimum temperature is expected to be much higher than the increase in maximum temperature, with maximum temperature expected to increase at most by 3.48 ºC during the 2090s, while minimum temperature is projected to increase by

6.33 ºC during the 2090s. The maximum rise in both minimum and maximum temperatures is projected by MIROC-ESM.

Fig 5. Maximum average annual temperature anomalies at the Jiri station with respect to the baseline period (1975 – 2004) for different GCMs.

4.3 Hydrological Modeling

The ArcSWAT 2012 model was used to simulate the hydrological processes under present and future climatic conditions. To delineate the watershed, an outlet was defined at the Busti station of the Tamakoshi River. This resulted in the creation of 66 sub-basins and 828 HRU (Hydrological Response unit) units. HRU is the smallest unit of a basin and is a combination of unique land features, soil types, and slope classification. Calibration and validation were carried out at the two outlets of the basin in the SWAT model. Initially, calibration and validation were done at the intake of the dam site. Six years of streamflow data, from 2001 to 2006, at the inlet of the dam, which is under the NEA network, was available. Four years of streamflow data, from 2001 to 2004, was used for calibration and two years, from 2005 to 2006, for validation (Fig. 6). In the next step, streamflow data of the outlet of the basin from 2000 to 2008 was used for calibration and validation. The streamflow data from 2004 to 2008 was used for the calibration of the model, and the streamflow data from 2000 to 2001 was used for validation (Fig. 7). A warm up period of 3 years, from 2001 to 2003, was used for calibration while a warm up period of 2 years, from 1998 to 1999, was used for the validation of the model. A sufficient warm up period is necessary to establish appropriate initial conditions for groundwater and soil water storage (Fontaine et al., 2002).

Fig. 6. Daily observed and simulated streamflow at the Busti station, the outlet of the watershed, after calibration (2004 – 2008) and validation (2000 – 2001).

Fig. 7. Daily observed and simulated streamflow at the Lamabagar station after calibration (2001 – 2004) and validation (2005 – 2006).

Fourteen model parameters were modified for the calibration of the SWAT model (Table 5). Temperature lapse rate and precipitation lapse rate play a significant role in adjusting the orographic distribution of the temperature and precipitation of the basin and were found to be the most sensitive. Hydraulic conductivity and curve number are other important parameters, and were found to be the most sensitive after the temperate lapse rate parameter. Temperature lapse rate was adjusted to the value of -5.5 ºC/km from its default value of zero (Khadka et al., 2014). The calibrated model seemed to have under-predicted some peak values during the monsoon period. The base flow was very well projected for both, the calibration and validation periods. The base flow alpha factor (Alpha_BF) is an important parameter to adjust the base flow. SOL_AWC (available water capacity of the soil) and SOL_K (saturated hydraulic conductivity) are other two sensitive soil parameters which were calibrated for the model. Auto-calibration, along with manual adjustments, was preferred for calibration in SWAT because of the involvement of a large set of parameters, including snowmelt parameters.

Table 5 Calibrated parameters, sensitivity analysis, and their default values for the SWAT model's simulations.

The simulated streamflow from the model showed a good match with the observed data and the performance of the model was evaluated using four statistical parameters: Nash Sutcliffe

Coefficient (NSE), coefficient of determination (R^2), RMSE observations Standard Deviation Ratio (RSR), and Percent Bias (PBIAS) (Table 6).

Table 6 The model's performance to simulate daily streamflow during the calibration period (2004 – 2008) and the validation period (2000 – 2001) at the Busti station, watershed outlet, and the Lamabagar station.

As for the daily data, the model showed good performance during the calibration and validation at the two outlets of the basin. At the Busti station, the outlet of the watershed, the model showed very good performance with an NSE value of 0.76 during the calibration period of 5 years and 0.84 during the validation period of 2 years. The coefficient of determination (R^2) was 0.76 for calibration and 0.85 for validation. Percent bias was negative during calibration, which indicates the model's overestimation, whereas the percent bias was positive during validation, which indicates the model's underestimation bias (Gupta et al., 1999).

4.4 Impact of Climate Change on Streamflow

The impact of climate change on the streamflow of the river at the intake of the dam site of the Tamakoshi basin was analyzed for three GCMs and two RCP scenarios in the future, as discussed earlier. Changes in precipitation patterns and intensity, along with change in temperature, can cause significant changes in the streamflow of a river. The changes in streamflow in the study area were compared with the streamflow of the baseline period of the intake dam site, as obtained from the SWAT model. Changes in the streamflow during the dry season show less uncertainty than the changes during the wet season, as the streamflow in

the river is significantly higher during the monsoon season as compared to the dry season. MRI-CGCM3 shows higher intensity of monsoon precipitation, as compared to other GCMs. Projections from MPI-ESM-M GCM show a decrease in precipitation during the future periods, due to which the streamflow in the river also shows decreasing projection.

All the three chosen GCMs show both increase as well as decrease in average monthly flow. Fig. 8 illustrates the comparison of streamflow in the future periods for different GCMs and also the comparison of these values with the baseline streamflow at the intake dam site. The decrease in dry season flow is more pronounced in the case of MIROC-ESM and MPI-ESM-M. MRI-CGCM3 projects an increase in winter flow during the 2030s and the 2060s under the RCP 4.5 scenario and during the 2030s and the 2090s under the RCP 8.5 scenario. However, the GCM expects a decrease in winter flow during the 2090s under the RCP 4.5 scenario and during the 2060s under the RCP 8.5 scenario. For MRI-CGCM3, the decrease in flow ranges from -0.43% in the month of April during the 2030s under the RCP 4.5 scenario to a maximum decrease in streamflow (above 17%) in the winter season during the 2090s under the RCP 4.5 scenario. Maximum increase in streamflow, by 84%, is expected to occur in the month of May during the 2090s under the RCP 8.5 scenario. The projection from MIROC-ESM shows that winter flow will decrease anywhere from -0.33% to -29.9% and summer flow will increase from +0.43% to +96.17% for all period and scenarios.

Fig. 8. Relative changes in streamflow at the Lamabagar station, the dam intake site for the future periods, based on (a) MRI-CGCM3, (b) MIROC-ESM, and (c) MPI-ESM-M GCMs relative to the baseline period (1975 – 2004).

The projection from MPI-ESM-M shows greater variation in the decrease in streamflow and less variation in the increase in streamflow, as compared to the other two GCMs. The

variation in the decrease in streamflow ranges from -4.62% to -37.83% while the variation in the increase in flow ranges from +0.03% to + 52.72%. An increase in streamflow is expected during the autumn season, with the maximum increase by 52.72% during the 2090s under the RCP 8.5 scenario. A decrease in streamflow is expected to occur during the other seasons, with maximum change, of over -36%, occurring in the winter season during the 2090s under the RCP 8.5 scenario.

4.5 Impact of Climate Change on Hydropower Production

Due to the variations in temperature and precipitation, the river's discharge is also expected to change with time and consequently will affect the production of hydropower as well. The mean flow at the intake of the dam site was found to be 60 m^3/s for the historical period. However, in the future, streamflow is projected to change due to variations in temperature and precipitation. Three GCMs (MIROC-ESM, MRI-CGCM3, and MPI-ESM-M) under two scenarios (RCP 4.5 and RCP 8.5) were used to assess the impact of climate change on hydropower production by the Upper Tamakoshi Hydropower Project. The average annual energy generation of this project is estimated to be 2281 GWh. The energy production of 2281 GWh is based on an artificially extended mean flow at the intake dam site. The artificially extended mean flow is based on three years of mean flow (2001 – 2003) at the intake dam site, which is 67.2 m^3/s. However, to analyze the impact of climate change on hydropower production in the future, the expected energy generation during the baseline period (1975 – 2004) was calculated based on the streamflow obtained from the SWAT model. The estimated historical energy production was found to be 1963 GWh only, with a mean streamflow of 60 m^3/s.

Table 7 illustrates the changes in energy production in the future, as compared to the baseline energy production of 1963 GWh, for different GCMs. Two GCMs, MIROC-ESM and MRI-CGCM3, show an increase in the average annual energy production, except for a decrease in energy production by 0.5% during the 2030s under the RCP 4.5 scenario with MIROC-ESM. Maximum energy production, an increase by 15.8%, is expected to occur during the 2090s under the RCP 8.5 scenario with MRI-CGCM3. MPI-ESM-M projects a decrease in average annual energy production, except for an increase in energy production (by 2.6%) during the 2060s under the RCP 4.5 scenario. MPI-ESM-M expects maximum decrease in energy production, by 7.6%, during the 2030s under the RCP 8.5 scenario. This decrease in energy production is expected from MPI-ESM-M's projections due to the estimated decrease in average annual precipitation in the future, leading to a decrease in the streamflow.

Table 7 Comparison of projected energy generation in the future, relative to the baseline energy production of 1963 GWh for different GCMs.

When the expected energy production in the future period is compared with the expected baseline energy production of 2281 GWh, all the three GCMs show decrease in energy production; the decreases range from -0.4% up to a maximum reduction by 20.5% (Table 8). MPI-ESM-M shows maximum reduction of energy production for all cases and scenarios.

Table 8 Comparison of projected energy generation in the future, relative to the baseline energy production of 2281 GWh, based on different GCMs.

4.6 Risk Analysis

The risk analysis of climate change on hydropower production was performed by calculating the percentage failures associated with the different values of annual energy production (E) for different periods and scenarios using three GCMs. Fig. 9 demonstrates the evolution of the risk values for different future periods: the 2030s (2015 – 2039), the 2060s (2040 – 2069), and the 2090s (2070 - 2099).

Fig. 9. Risk in annual energy production for the periods of the 2030s, the 2060s, and the 2090s under RCP 4.5 and RCP 8.5 scenarios for different GCMs.

The results show an increase in the risk percentage with an increase in the annual energy production for all the three GCMs and RCP scenarios. The increase or decrease in the risk value depends upon the streamflow of the river and the monthly energy production. The risk value tends to decrease with increase in streamflow and increase in energy production. Although there is an overall increase in the streamflow and energy production in the future periods for MIROC-ESM and MRI-CGCM3, energy production levels during some dry seasons will not be achieved as expected in the designed or baseline periods. As a result, a risk occurs in those periods in which the energy is not produced as expected. MPI-ESM-M expects a decrease in monthly as well as annual energy production in the future periods. Therefore, the risk percentage of failure is higher during the future periods for MPI-ESM-M. It is evident from Fig. 9 that there is a trend of increase in the risk percent with the increase in energy production levels, as discussed earlier. However, no risk is projected for the future due to climate change for some scenarios and periods for MRI-CGCM3. The risk of failure is projected to be zero (i.e. no risk) during the 2060s under the RCP 4.5 scenario and during the 2090s under the RCP 8.5 scenario. All three GCMs show percentage risk associated due to

the impact of climate change on the hydropower production of the Upper Tamakoshi Hydropower Project. MRI-CGCM3 expects the least percentage of risk during the future periods with one exception: during the 2090s under the RCP 4.5 scenario. The risk percentage for MIROC-ESM varies from a minimum value of 1.06% during the 2090s under RCP 4.5 to 2.52% during the 2030s under the same scenario. MPI-ESM-M shows the maximum occurrence of risk, as compared to other GCMs, since energy production is expected to decrease in the future for this GCM. The projections show that the least percentage of risk during the 2060s is under RCP 4.5, with 1.81%. The risk percentage for other scenarios and periods varies from 3.37% to 6.63%, with the maximum percentage of risk expected to occur during the 2030s under the RCP 8.5 scenario.

The risk values in the future are significantly higher when the expected energy production is compared with the baseline energy production of 2281 GWh. The risk percentage varies from a minimum value of 0.88% to a maximum of 13.24%. Fig. 10 shows the percentage risk associated with hydropower production in the future periods, relative to the baseline production of 1963 GWh and 2283 GWh, for different GCMs and RCP scenarios.

Fig. 10. Percentage risk associated with hydropower production in future periods, relative to the baseline production of 1963 GWh (left) and 2283 GWh (right), for different GCMs and RCP scenarios.

The risk values obtained from this research can be categorized into different levels of performance based on the change in the performance indicator. Grijsen et al. (2013) defined risk levels based on the change in the percentage interval of the performance indicators for the production of hydropower. Indicators such as guaranteed energy production during the dry season and total energy production can be considered for climate risk analysis (Grijsen et

al., 2013). The risk level is categorized thus: mild risk when the change in the performance indicator is below 10% and moderate if the change is between 10 and 20%. The risk is considered to be significant if the risk percentage is greater than 20%. According to the risk levels defined, mild risk is expected in the future energy production of the Upper Tamakoshi Hydropower Project, since the energy production drops for all GCMs and scenarios compared to the baseline energy production of 1963 GWh. Mild to moderate levels of risk were found when the future energy production was compared with the baseline energy production of 2281 GWh. The level of risk can also be represented in terms of monetary units (Fig. 11). The higher the risk, the higher will be the risk in terms of economic loss. The risk related to economic loss was calculated based on an initial assumption of the export price of energy production at 2.5 US Cents (USc) per KWh.

Fig. 11. Risk in terms of USD (in millions) associated with hydropower production in the future periods, relative to the baseline production of 1963 GWh (left) and 2281 GWh (right), for different GCMs and RCP scenarios.

The current level of risk is based on the maximum capacity of 456 MW from the designed streamflow of 66 m^3/s. The risk levels were analyzed for different levels of design capacity of the hydropower plant. Fig. 12 shows that the risk percentage of energy production tends to decrease with an increase in the installed capacity of the hydropower plant for all three GCMs. The installation of a higher capacity turbine can reduce the percentage risk in the future energy production. However, this increase in turbine capacity can affect the cost benefit ratio and net profit from the project. Proper economic analysis and optimization of the installed capacity and incorporation of the percentage risk level is required before

recommending the optimized installed capacity of the turbine. The analysis should also take into account the effects of climate change.

Fig. 12. Average percentage risk associated with different levels of the installed capacity of the hydropower plant for different GCMs.

5. Conclusion

This study assessed the impact of climate change, and the associated risks, on the energy production of the Upper Tamakoshi Hydropower Project which is located in the Tamakoshi basin of Nepal. The Tamakoshi basin is one of the sub-basins of the Koshi basin in Nepal. This basin has very limited hydro-meteorological stations. Despite that, the hydrological model SWAT performed well in simulating the streamflow of the basin. The projection of precipitation for the future periods was found to be uncertain and varied, without any discernible trend, seasonally with different GCMs. The projections from MIROC-ESM and MRI-CGCM3 show an increase in precipitation. On the contrary, MPI-ESM-M projects a decrease in precipitation. The selection of a GCM can be a contributing factor in the uncertainty in the projection of precipitation in a basin. On the other hand, temperature is projected to increase for all GCMs and under all scenarios though the magnitude of projection varies for different GCMs. Increase in minimum temperature was found to be higher than in maximum temperature. The results from this study show significant changes in the streamflow in the study basin due to variations in projected temperature and prec ipitation, as compared to the baseline period. The projected precipitation varies from -8% to +24.8%, which is expected to alter the streamflow, ranging from -37.83% to +47%. Based on the streamflow output, the risk was calculated for the projected energy production with respect to the baseline energy production of 1963 GWh and 2281 GWh. Mild risk, ranging

from 0.69% to 6.63%, was computed by comparing the projections to the baseline production of 1963 GWh. Mild to moderate risk, varying from 2.73% to 13.4%, can be expected for the baseline production of 2281 GWh. The impact of projected temperature and precipitation on streamflow and hydropower generation varies significantly among the different GCMs. The risk associated with energy production also shows significant variation. The uncertainty in the projection of streamflow, arising due to the choice of GCM, should be taken into consideration by the policy makers and planners before they implement the adaptation measures to deal with the changing climate conditions and, therefore, be able to properly address the anticipated risk to be incorporated before appropriate measures are taken.

References

Babel, M. S., Bhusal, S. P., Wahid, S. M., and Agarwal, A.: Climate change and water resources in the Bagmati River Basin, Nepal, Theoretical and applied climatology, 115, 639-654, 2014

Baede, A. P. M., Ahlonsou, E., Ding, Y., and Schimel, D. S.: The climate system: an overview, in: Climate Change 2001: impacts, adaptation and vulnerability, Cambridge University Press, 87-98, 2001.

Bala, G.: Digesting 400 ppm for global mean CO2 concentration, Current science, 104, 1471-1471, 2013.

Bharati, L., Gurung, P., Jayakody, P., Smakhtin, V., and Bhattarai, U.: The projected impact of climate change on water availability and development in the Koshi Basin, Nepal, Mountain Research and Development, 34, 118-130, 2014.

Department of Electricity Development, Ministry of Energy, Government of Nepal (DOED): http://www.doed.gov.np/operating_projects_ hydro.php, last access: 13 April 2015.

Giorgetta, M. A., Jungclaus, J., Reick, C. H., Legutke, S., Bader, J., Böttinger, M., and Stevens, B.: Climate and carbon cycle changes from 1850 to 2100 in MPI-ESM simulations for the Coupled Model Intercomparison Project phase 5, Journal of Advances in Modeling Earth Systems, 5, 572-597, 2013.

Grijsen, J.: Understanding the Impact of Climate Change on Hydropower: the case of

Cameroon, 2014.

Gudmundsson, L., Bremnes, J. B., Haugen, J. E., and Engen-Skaugen, T.: Technical Note: Downscaling RCM precipitation to the station scale using statistical transformations–a comparison of methods, Hydrology and Earth System Sciences, 16, 3383-3390, 2012.

Hamlet, A. F., Salathé, E. P., and Carrasco, P.: Statistical downscaling techniques for global climate model simulations of temperature and precipitation with application to water resources planning studies, The Columbia Basin Climate Change Scenarios Project (CBCCSP) report, 2010.

Khadka, D., Babel, M. S., Shrestha, S., and Tripathi, N. K.: Climate change impact on glacier and snow melt and runoff in Tamakoshi basin in the Hindu Kush Himalayan (HKH) region, Journal of Hydrology, 511, 49-60, 2014.

Mimikou, M. A., and Baltas, E. A.: Climate change impacts on the reliability of hydroelectric energy production, Hydrological Sciences Journal, 42, 661-678, 1997.

Moriasi, D. N., Arnold, J. G., Van Liew, M. W., Bingner, R. L., Harmel, R. D., and Veith, T. L.: Model evaluation guidelines for systematic quantification of accuracy in watershed simulations, Trans. Asabe, 50, 885-900, 2007.

Neitsch, S. L., Arnold, J. G., Kiniry, J. R., Williams, J. R., and King, K. W.: SWAT Theoretical documentation version 2009. Blackland Research Center, Temple, TX., 2009.

Robinson, P.J.: Climate change and hydropower generation, Int. J. Climatol, 17, 983-996, 1997.

Shea, J. M., Immerzeel, W. W., Wagnon, P., Vincent, C., and Bajracharya, S.: Modelling glacier change in the Everest region, Nepal Himalaya: The Cryosphere Discussions, 8, 5375-5432, 2014.

Shrestha, A. B., and Aryal, R: Climate change in Nepal and its impact on Himalayan Glaciers, Regional Environmental Change, 11(1), 65-77, 2011.

Shrestha, R. B.: Power Sector and Hydropower Development in Nepal, Hydro Nepal: Journal of Water, Energy and Environment, 16, 18-22, 2015.

Shrestha, S., Khatiwada, M., Babel, M. S., and Parajuli, K: Impact of Climate Change on River Flow and Hydropower Production in Kulekhani Hydropower Project of Nepal, Environmental Processes, 1(3), 231-250, 2014.

Stocker, T. F., Qin, D., Plattner, G. K., Tignor, M., Allen, S. K., Boschung, J., and Midgley, P.M.: Climate change 2013: The physical science basis. Intergovernmental Panel on Climate Change, Working Group I Contribution to the IPCC Fifth Assessment Report (Cambridge Univ Press, New York), 2013.

Teutschbein, C., Wetterhall, F., and Seibert, J.: Evaluation of different downscaling techniques for hydrological climate-change impact studies at the catchment scale, Climate Dynamics, 37(9-10), 2087-2105, 2011.

USDA: Soil Conservation Service National Engineering Handbook, Section 4: Hydrology. Washington DC, 1969.

Watanabe, S., Hajima, T., Sudo, K., Nagashima, T., Takemura, T., Okajima, H., et al.: MIROC-ESM 2010: Model description and basic results of CMIP5-20c3m experiments, Geoscientific Model Development, 4, 845-872, 2011

Yukimoto, S., Adachi, Y., Hosaka, M., Sakami, T., Yoshimura, H., Hirabara, M., and Kitoh, A.: A new global climate model of the Meteorological Research Institute: MRI-CGCM3-model description and basic performance, 気象集誌. 第 2 輯, 90, 23-64, 2012.

Table 1 Hydro-meteorological stations of in the Tamakoshi basin used in the study.

Station Name	Type of Station	Latitude	Longitude	Elevation (masl)	Year	Source
Charikot	Precipitation	27°40'	86°03'	1940	1959-2013	DHM
Jiri	Agro meteorology	27°38'	86°14'	2003	1961-2013	DHM
Lamabagar	Hydrological	27°54'	86°16'	1965	2001-2006	DHM
Busti	Hydrological	27°38'	86°05'	849	1970-2013	NEA

Table 2 GCMs, their sources, resolutions, vintage and data sources used in the study.

GCMs	Resolution	Institute	Vintage	References
MIROC-ESM	2.81° × 2.81°	University of Tokyo	2010	Watanabe et al., 2011
MRI-CGCM3	3.75° × 3.75°	MRI, Japan	2011	Yukimoto et. al., 2012
MPI-ESM-M	1.87° × 1.87°	MPI, Germany	2013	Giorgetta et. al., 2013

Table 3 Evaluation of bias correction for precipitaiton data of MIROC-ESM, MRI-CGCM3, and MPI-ESM-M GCMs for the Charikot Station.

Charikot Station		Observed	MIROC-ESM		MRI-CGCM3		MPI-ESM-M	
			Raw	Corrected	Raw	Corrected	Raw	Corrected
Precipitation (mm)	SD	206.78	111.57	217.4	119.69	226.67	201.9	219.5
	R^2		0.43	0.70	0.43	0.66	0.58	0.67
	RMSE		170.09	122.12	186.83	135.04	147.3	135.13

Table 4 Evaluation of bias correction for precipitation, minimum temperature, and maximum temperature data of MIROC-ESM, MRI-CGCM3, and MPI-ESM-M GCMs for the Jiri Station.

Jiri Station		Observed	MIROC-ESM		MRI-CGCM3		MPI-ESM-M	
			Raw	Corrected	Raw	Corrected	Raw	Corrected
Precipitation (mm)	SD	227.73	111.57	235.63	119.69	248.89	201.9	240.5
	R^2	-	0.44	0.73	0.38	0.63	0.62	0.7
	RMSE	-	194.54	125.41	220.76	154.58	159.5	136.15
Min Temp. (℃)	SD	6.76	6.44	7.37	6.18	6.84	7.19	6.81
	R^2	-	0.87	0.90	0.88	0.92	0.86	0.93
	RMSE	-	3.72	2.01	2.80	1.89	9.02	2.89
Max Temp. (℃)	SD	4.17	5.09	3.92	7.44	3.78	7.59	3.97
	R^2	-	0.69	0.85	0.69	0.72	0.55	0.69
	RMSE	-	3.81	1.87	4.64	2.32	10.44	2.42

Table 5 Calibrated parameters, sensitivity analysis, and their default values for the SWAT model's simulations.

Input Parameters	Description	Rank	Final Fitted Value	Lower and Upper Bound
TLAPS	Temperature Lapse Rate (ºC/km)	1	-5.5	±50
CH_K1	Effective hydraulic conductivity in tributary channel (mm/hr)	2	79	0-300
SFTMP	Snowfall temperature (ºC)	3	0.2	±5
CN2	Initial runoff SCS curve number	4	60-85	35-98
PLAPS	Precipitation Lapse Rate (mm/Km)	5	±150	±500
SOL_K	Saturated hydraulic conductivity (mm/hr)	6	190	0-2000
SMFMX	Maximum melt rate for snow during the year (mm/ºC-day)	7	9	0-10
CH_K2	Effective hydraulic conductivity in main channel (mm/hr)	8	267	0 - 500
Alpha_BF	Base -flow alpha factor (days)	9	0.36	0-1
SMTMP	Snowmelt temperature (ºC)	10	2	±5
SOL_AWC	Available water capacity of the soil (mm/mm)	11	0.68	0-1
GW_Delay	Groundwater Delay (days)	13	337	0-500
CH_N2	Manning n value for main channel	14	0.288	0-0.3
SMFMN	Minimum melt rate for snow during the year (mm/ºC-day)	15	7	0-10

Table 6 The mModel's performance to simulate of daily streamflow during the calibration period (2004 -– 2008) and the validation period (2000 -– 2001) at the Busti station, watershed outlet, and the Lamabagar station.

Statistics	Busti Station		Lamabagar Station	
	Calibration	Validation	Calibration	Validation
NSE	0.76	0.84	0.71	0.78
R^2	0.76	0.85	0.8	0.82
PBIAS	-1.69%	5.24%	-7.73%	14.25%
RSR	0.53	0.28	0.54	0.33

Table 7 Comparison of future projected energy generation in the future, relative to the baseline energy production of 1963 GWh for different GCMs.

GCMs	Scenario	Baseline Energy	Energy Generated (GWh)			% Difference		
			2030s	2060s	2090s	2030s	2060s	2090s
MIROC-ESM	RCP 4.5	1963 GWh	1954.1	2064.8	2088.7	-0.5	5.2	6.4
	RCP 8.5		2024.7	2012.2	2045.9	3.1	2.5	4.2
MRI-CGCM3	RCP 4.5		1978.4	2123.1	1963.6	0.8	8.2	0.03
	RCP 8.5		1991.7	2009.5	2272.9	1.5	2.4	15.8
MPI-ESM-M	RCP 4.5		1845.2	2014.0	1952.8	-6.0	2.6	-0.5
	RCP 8.5		1814.0	1869.8	1901.9	-7.6	-4.7	-3.1

Table 8 Comparison of future projected energy generation in the future, relative to the baseline energy production of 2281 GWh, based on different GCMs.

GCMs	Scenario	Baseline Energy	Energy Generated (GWh)			% Difference		
			2030s	2060s	2090s	2030s	2060s	2090s
MIROC-ESM	RCP 4.5	2281 GWh	1954.1	2064.8	2088.7	-14.3	-9.5	-8.4
	RCP 8.5		2024.7	2012.2	2045.9	-11.2	-11.8	-10.3
MRI-CGCM3	RCP 4.5		1978.4	2123.1	1963.6	-13.3	-6.9	-13.92
	RCP 8.5		1991.7	2009.5	2272.9	-12.7	-11.9	-0.4
MPI-ESM-M	RCP 4.5		1845.2	2014.0	1952.8	-19.1	-11.7	-14.4
	RCP 8.5		1814.0	1869.8	1901.9	-20.5	-18.0	-16.6

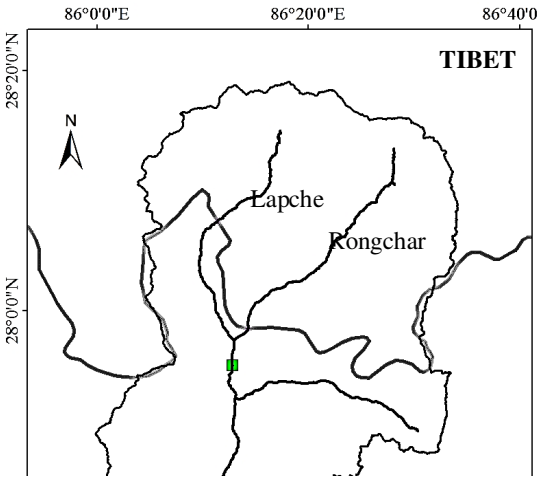

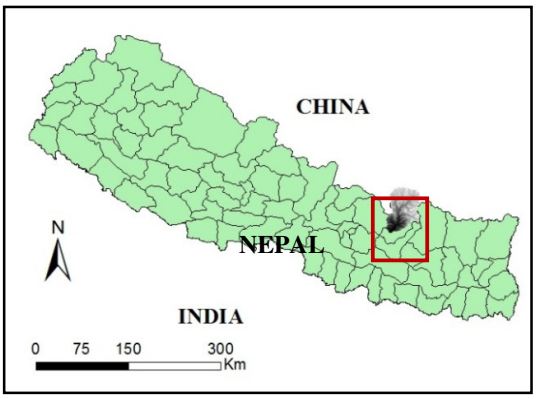

Fig. 1. Location map of the Tamakoshi basin showing with its hydrological and meteorological stations.

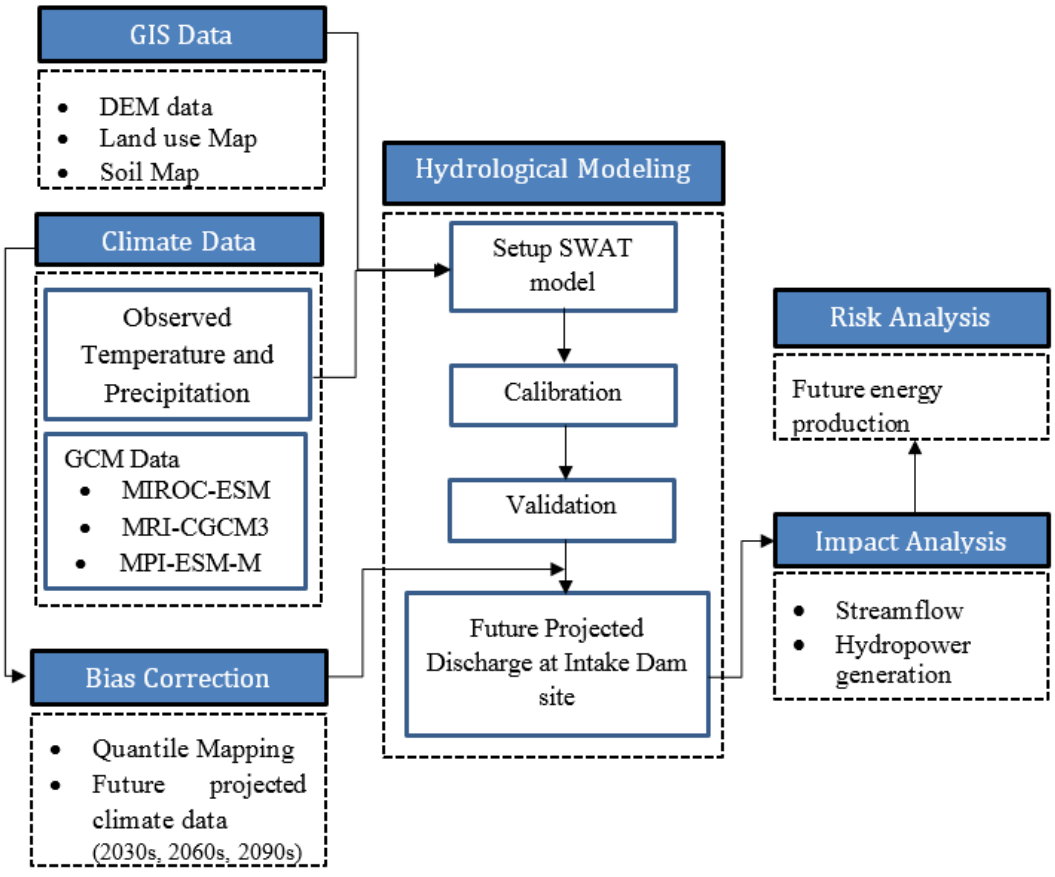

Fig. 2. The methodology adopted for the study.

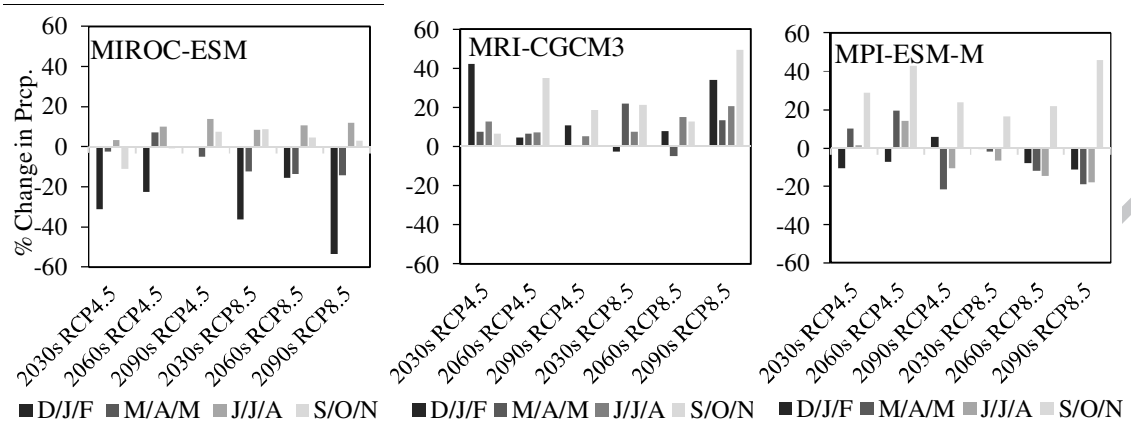

Fig. 3. Percentage change in future projected precipitation at the Charikot station with respect to the baseline period (1975 – 2004) for different GCMs.

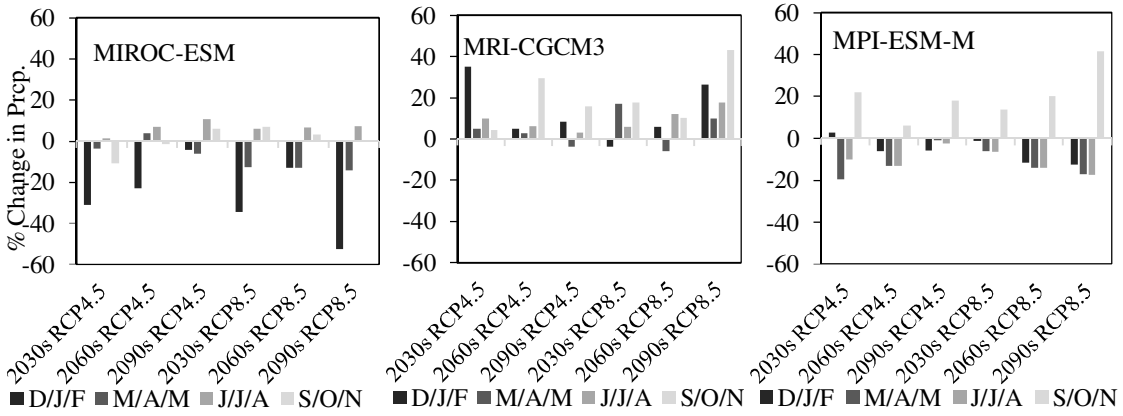

Fig. 4. Percentage change in future projected precipitation for the future at the Jiri station with respect to the baseline period (1975 -– 2004) for different GCMs.

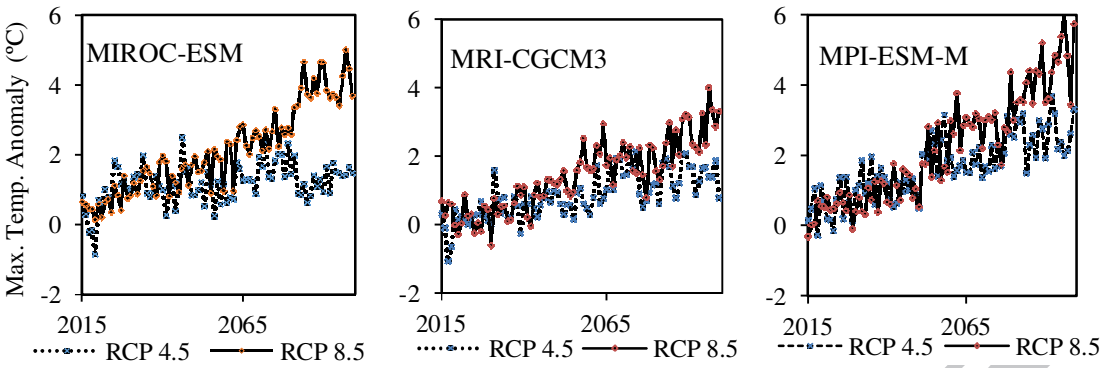

Fig. 5. Maximum average annual temperature anomalies y ofat the Jiri station with respect to the baseline period (1975 –– 2004) for different GCMs.

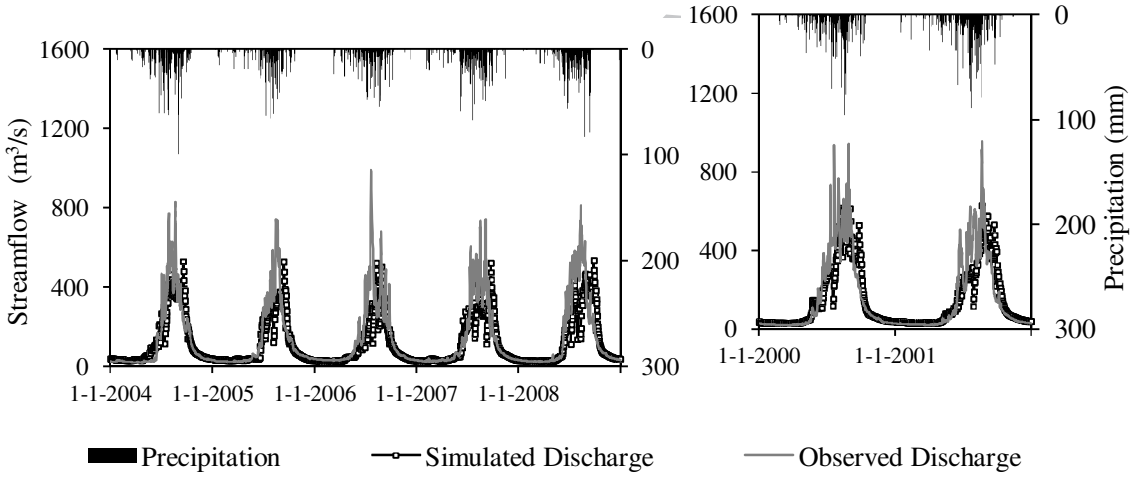

Fig. 6. Daily observed and simulated streamflow at the Busti station, the outlet of the watershed, after calibration (2004 –– 2008) and validation (2000 –– 2001).

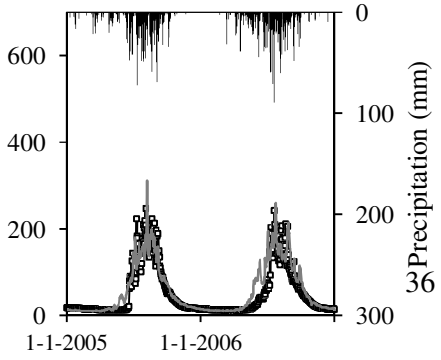

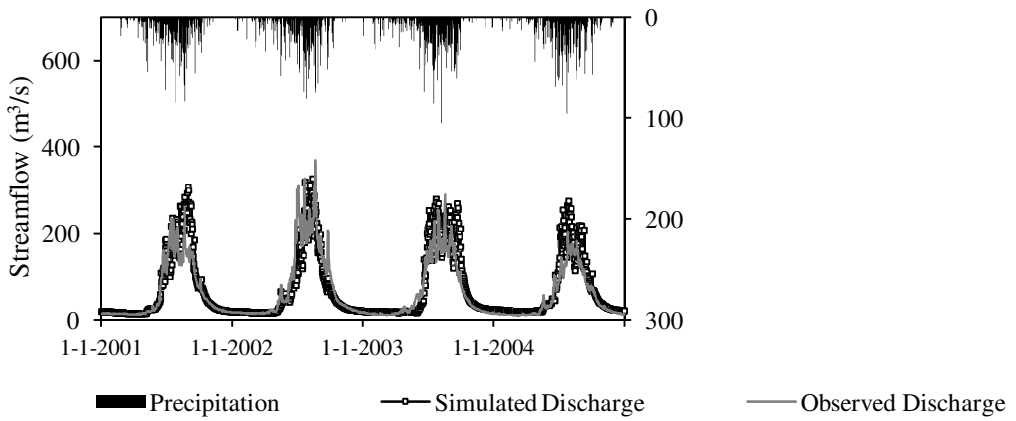

Fig. 7. Daily observed and simulated streamflow at the Lamabagar station after calibration (2001 –– 2004) and validation (2005 –– 2006).

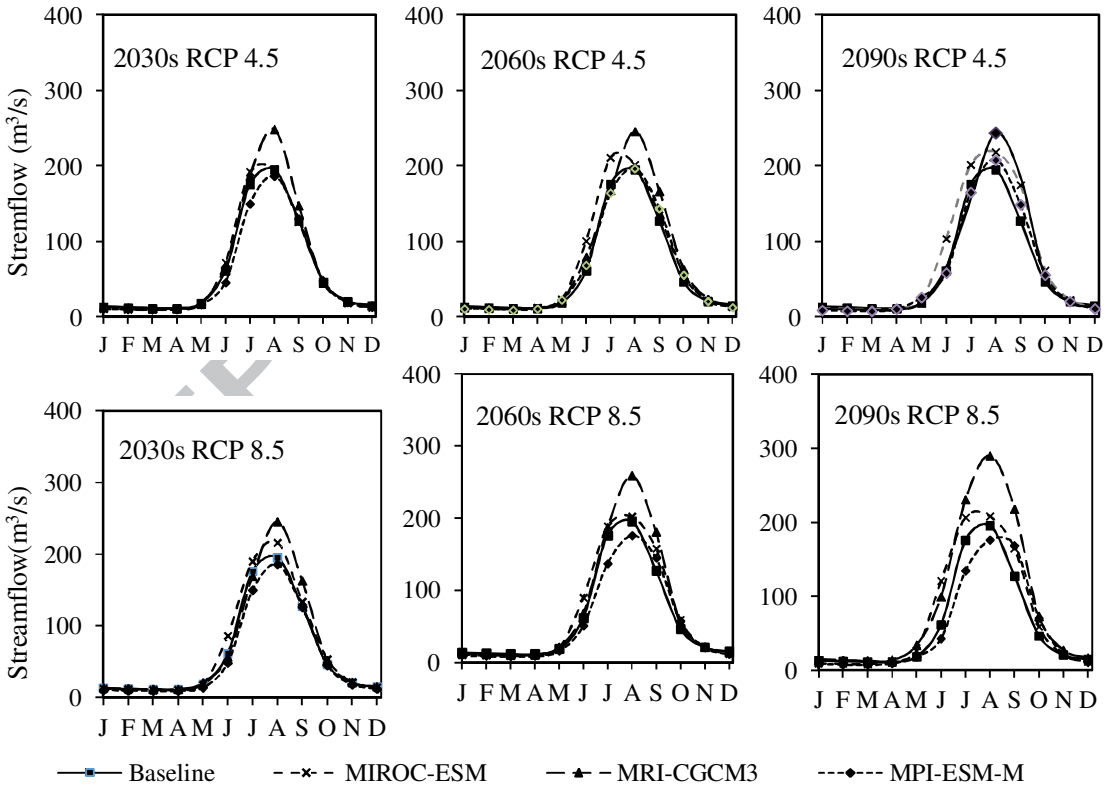

Fig. 8. Relative changes in streamflow at the Lamabagar station, the dam intake site for the future periods, based on (a) MRI-CGCM3, (b) MIROC-ESM, and (c) MPI-ESM-M GCMs relative to the baseline period (1975 -– 2004).

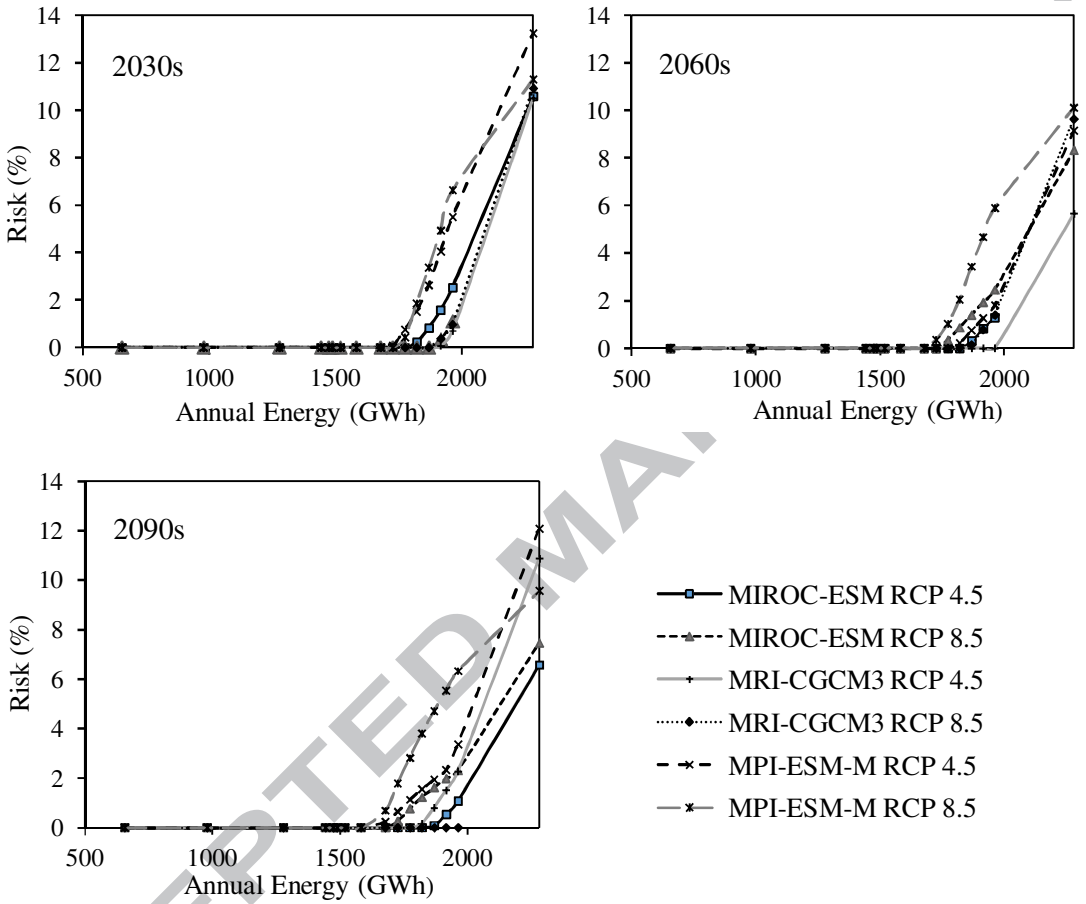

Fig. 9. Risk vs in annual energy production for the periods of the 2030s, the 2060s, and the 2090s for under RCP 4.5 and RCP 8.5 scenarios for different GCMs.

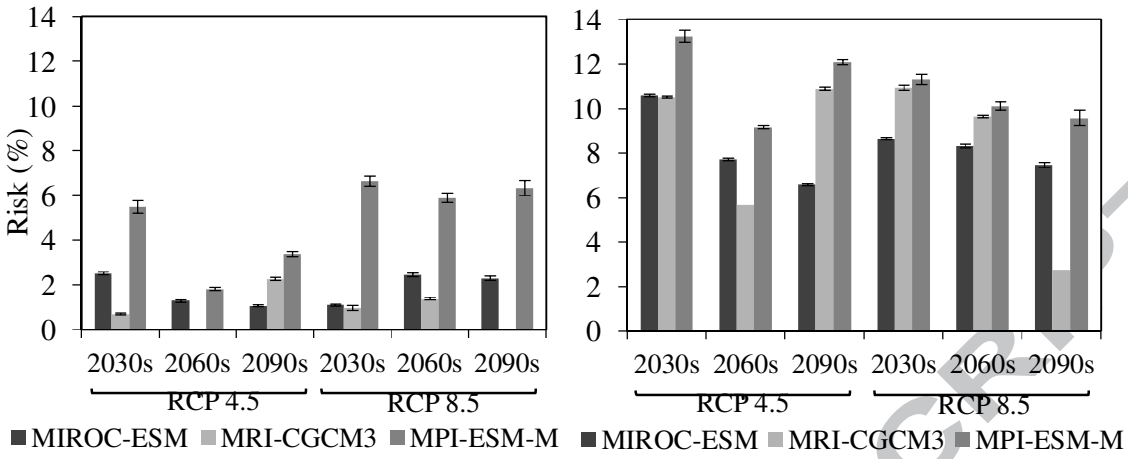

Fig. 10. Percentage risk associated with hydropower production in future periods, relative to the baseline production of 1963 GWh (left) and 2283 GWh (right), for different GCMs and RCP scenarios.

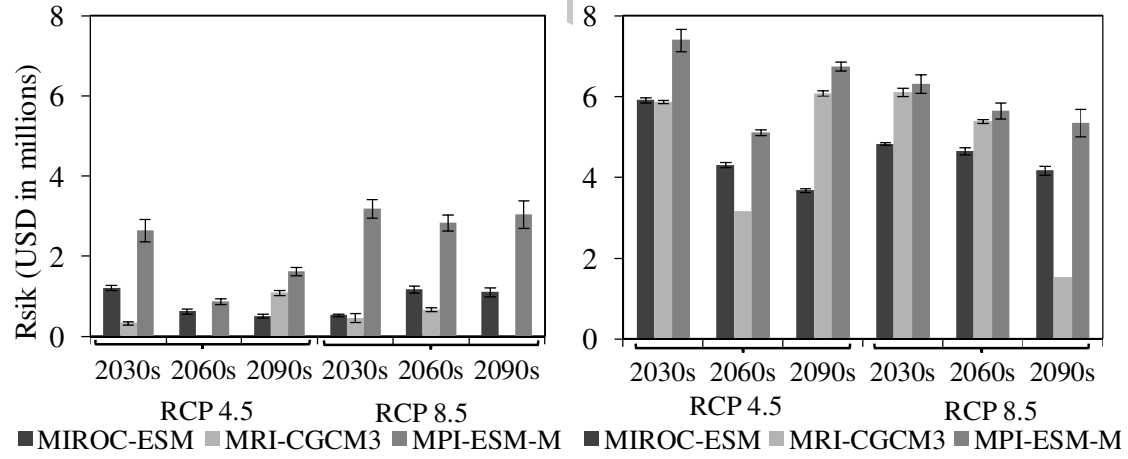

Fig. 11. Risk in terms of USD (in millions) associated with hydropower production in the future periods, relative to the baseline production of 1963 GWh (left) and 2281 GWh (right), for different GCMs and RCP scenarios.

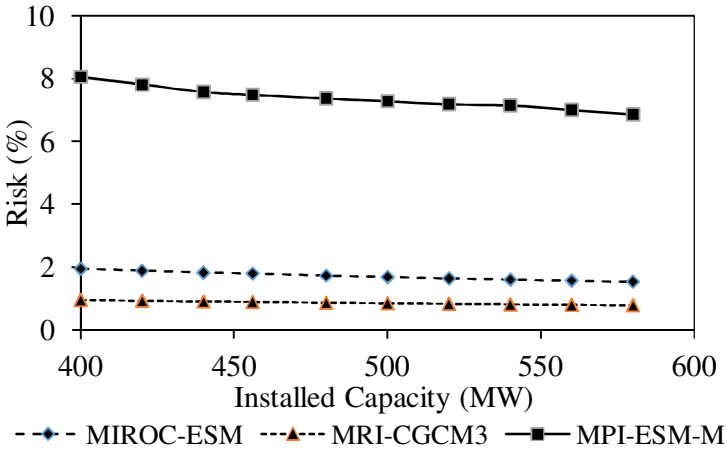

Fig. 12. Average percentage risk associated with different levels of the installed capacity of the hydropower plant for different GCMs.